Spectral method study of domain coarsening

David J. Horntrop*

Department of Mathematical Sciences, New Jersey Institute of Technology, Newark, New Jersey 07102, USA

(Received 23 October 2006; revised manuscript received 15 January 2007; published 10 April 2007)

The self-organization of particles in a two phase system in the coexistence region through a diffusive mechanism is known as Ostwald ripening. The late stage of Ostwald ripening is studied here through the use of a mesoscopic model in conjunction with a special configuration that allows for the direct measurement of system characteristics such as domain size. The mesoscopic model is a stochastic partial integrodifferential equation and is studied through the use of recently developed and benchmarked spectral schemes. The size of the growing region is not observed to increase as a power law in this model during the late stages of self-organization in contrast to the power law growth observed in simulations of the earlier stages of self-organization. The results included here also demonstrate the effect of adjusting the interparticle interaction on the morphological evolution of the system.

DOI: 10.1103/PhysRevE.75.046703 PACS number(s): 02.70.−c, 05.10.−a, 05.40.−a

I. INTRODUCTION

An important phenomenon is the coarsening that is observed in a two phase system in which mass is transported through diffusion. This phenomenon is commonly referred to as Ostwald ripening in honor of an early pioneer in this field. The evolution of this system is driven to minimize the free energy, resulting in a reduction of the overall interfacial area of the system. Larger regions of the minority phase grow at the expense of the smaller regions. The number of regions decreases in time while the average size of the remaining regions increases due to the conservative nature of diffusional transport. Eventually, only a single region remains.

Ostwald ripening has been quite difficult to study at least in part due to its inherently multiscale nature. The observable, macroscale behavior of this system is strongly impacted by molecular level behavior. One of the earliest successful theories regarding Ostwald ripening was derived independently by Lifshitz and Slyozov [1] and Wagner [2] and is often referred to as the LSW theory. Assuming spherical particles which do not interact, in the limit of zero volume fraction of the minority phase, it was asymptotically determined that the domain size of a typical cluster of particles evolves according to a temporal power law. The LSW growth law can be obtained by a simple scaling argument [3], though more complete derivations appear in [1,2,4–7]. The LSW growth law is

$$R \sim t^{1/3}, \tag{1}$$

where R denotes the size of a typical cluster and t is time.

While this result is well known to be of great importance in understanding Ostwald ripening, the shortcomings of the LSW theory are also widely recognized. One of the greatest difficulties of the LSW theory is the assumption of no interparticle interactions. Intuitively, one would expect that the coarsening of a domain depends upon the size and proximity of other clusters; for example, an isolated cluster will behave quite differently than a cluster surrounded by other large clusters. The experimental results in [8] also demonstrate the importance of particle interactions during Ostwald ripening. A great deal of modeling has been done in an attempt to incorporate interparticle interactions in the framework of the LSW theory. The review articles in [5–7] describe and include references to this large body of work. This paper will focus on the recently derived mesoscopic models that explicitly include interparticle interactions [9–13].

Computation has traditionally played an important role in studies of Ostwald ripening. Boundary integral methods have often been used in studies of the LSW model [14–18]. A finite volume approach was used for a suitably reformulated version of the LSW model in [19] and [20]. However, most computational work related to Ostwald ripening has been based upon the Cahn-Hilliard field theory model. While there has been some use of finite element methods for the Cahn-Hilliard equation [21,22], most computational work has focused on the use of finite differences. Applying finite differences to the Cahn-Hilliard equation is rather difficult for a number of reasons. The appearance of fourth derivatives in the Cahn-Hilliard equation places rather severe restrictions on the choice of time step for numerical stability when time stepping is done using explicit methods. The discretization used must also respect the conservation of mass in the system. In spite of these difficulties, many useful results have been obtained [23–29].

In contrast to the macroscale models discussed above, Ostwald ripening can also be studied through microscale models that consider each individual particle in a system. The Ising spin exchange model is commonly used to study Ostwald ripening. The simplest means of computationally implementing this particle model is to use Kawasaki's algorithm [30]. In this method adjacent pairs of particles are selected at random as candidates for an exchange; the determination of whether or not the exchange occurs depends on the Metropolis probability. Typical results from such simulations appear in [3] and [31–33]. Such an approach is very computationally intensive especially when the system has become fairly well organized so that most adjacent pairs of particles have the same value thereby eliminating any possible effect of the exchange of that pair. Thus a great deal of computational resources are necessary to accomplish simulations for

*FAX: (973) 596-5591. Email address: horntrop@njit.edu

a long time with a large number of particles. Accordingly, many approximations and other speedups to Kawasaki's algorithm have been proposed [3,31–34]. While a great deal of improvement in efficiency has been accomplished by these efforts, long time simulations are still difficult to obtain using such particle based methods, though recently developed coarse-grained Monte Carlo methods which are applicable to a wide class of problems in addition to Ostwald ripening show a great deal of promise in both accuracy and efficiency [35,36].

In this paper mesoscopic models are used in a computational study of Ostwald ripening. These models are similar in nature to the field theory models but are derived directly from microscopic models. Earlier simulations of the mesoscopic model have demonstrated the validity of this as a model for Ostwald ripening [37,38]. In particular, domain growth as predicted by the LSW growth law in Eq. (1) at relatively early times was observed with a transition to an even faster growth at later times. The goal of this paper is to study a special configuration that represents the late stages of domain coarsening. In Sec. II, the mesosopic model that is an appropriate model for Ostwald ripening is described. Section III discusses the computational technique used in the simulation of the mesoscopic model. In Sec. IV, previously obtained simulation results are described and the reasons why a special configuration is needed to quantitatively study the late stages of domain coarsening are given. Also in Sec. IV, simulation results for the late stages of domain coarsening are given; the effect of changing the particle interaction length on the time scale of the late stages of the coarsening process is also described. Finally, conclusions and areas for further study are given in Sec. V.

II. DESCRIPTION OF MESOSCOPIC MODEL

Mesoscopic models are local mean field theories that are designed to bridge the gap between microscopic and macroscopic scales by directly incorporating microscopic level behavior in the macroscopic level. Since details of the derivation of this class of mesoscopic models have been given in [9–13], only a brief qualitative discussion will be given here. This class of mesoscopic models is derived through a coarse graining of the underlying microscopic system that does not require the introduction of artificial truncations. The average coverage is calculated over a ball with a radius that is small compared with the interaction radius, thereby averaging the small random fluctuations while still capturing spatial variations in the coverage. In passing to the limit of infinite interaction radius, an evolution equation of the average coverage can be derived that includes stochastic terms. Such an approach has been followed for various micromechanisms while insuring that the underlying Gibbs measure remains invariant, i.e., detailed balance is satisfied.

Mesoscopic models deserve study for a number of reasons. Certainly an extremely important feature of these models is the fact that the noise term in the equation arises as a result of a derivation rather than being introduced in an *ad hoc* fashion. Also, the fact that the mesoscopic model is a continuum model should allow for more efficient computer simulations as compared with the underlying particle model. In addition, the coupling of continuum models with other continuum models is much more straightforward than coupling of continuum models with particle models.

The mesoscopic model that is an appropriate model of Ostwald ripening is derived from the spin exchange (surface diffusion) mechanism and is given by the following stochastic partial integrodifferential equation:

$$u_t - D\nabla \cdot [\nabla u - \beta u(1-u)\nabla J_m * u] + \gamma \,\mathrm{div}[\sqrt{2Du(1-u)}dW(x,t)] = 0, \tag{2}$$

where u is the concentration of the minority phase, D is the diffusion constant, β is proportional to the inverse of the temperature of the underlying Ising model, J_m is the migration potential denotes convolution, γ is proportional to the interaction length of the particles, and dW represents a (white noise) process that is delta correlated in both space and time with

$$\langle dW(x,t)\rangle = 0$$

and

$$\langle dW(x,t)dW(x',t')\rangle = \delta(x-x')\delta(t-t'),$$

where the angular brackets are used to denote mean values. It is important to observe that the noise in Eq. (2) is multiplicative rather than the additive noise that is commonly added to deterministic models in an *ad hoc* manner. It is also noteworthy that the Cahn-Hilliard equation can be obtained from the deterministic version of Eq. (2) by a suitable rescaling and Taylor expansion and thus is a special case of this equation [13].

The model in Eq. (2) has many attributes that make it attractive for studying Ostwald ripening. There is theoretical and computational evidence of the validity of the mesoscopic model in Eq. (2). A large deviation principle argument has been given which shows that the probability that Eq. (2) differs from the underlying particle system decays exponentially [39,40]. Prior computational simulations of Eq. (2) have also exhibited power law growth similar to Eq. (1) at early stages of the self-organization [37]. Another useful feature of Eq. (2) is the explicit appearance of the interaction potential which transparently allows for the consideration of a wide variety of interparticle interactions.

A computational study of the mesoscopic model in Eq. (2) in a special situation which is similar to the late stages of self-organization is described in this paper. Numerical techniques for stochastic partial differential equations such as Eq. (2) have received limited attention in the literature as compared with deterministic equations. Some examples of techniques using finite differences appear in [41–45]. Stochastic finite elements are discussed in [46] and applied to stochastic partial differential equations driven by white noise in [47–50]. While these numerical methods could be used to simulate Eq. (2), the focus here is on spectral methods. While spectral methods have been used previously for stochastic partial differential equations with additive noise [51], their application for equations with multiplicative noise is novel [52]. There are a number of reasons why a spectral

method seems to be a particularly attractive computational approach for Eq. (2). The calculation of convolutions is straightforward and efficient in a spectral method. In [13] it was demonstrated for a deterministic mesoscopic model that spectral methods were much more accurate than finite difference methods for a comparable computational effort. When time stepping is done in Fourier space, spectral methods also allow for terms which become linear in Fourier space, such as diffusive terms, to be treated exactly using an integrating factor, thereby both increasing accuracy and directly reducing computational time. The integrating factor also eases stability restrictions on admissible time steps thus allowing the use of larger times steps than are numerically stable if the linear terms were not calculated exactly when one is using an explicit time stepping scheme [53].

III. DESCRIPTION OF SIMULATION METHOD

The numerical scheme that is used to study the mesoscopic model in Eq. (2) is based upon a generalization of spectral schemes for deterministic partial differential equations to the stochastic setting. For the sake of simplicity in the description of the numerical method here, it is assumed that the stochastic partial differential equation in Eq. (2) has only one spatial dimension. This method straightforwardly generalizes to higher spatial dimension as evidenced by the two spatial dimension results presented later in this paper.

Spectral schemes for deterministic evolution equations form the starting point for the development of spectral techniques for the simulation of solutions to Eq. (2). The solution of the equation is expanded in a Fourier series in the spatial component

$$u(x,t) = \sum_{\xi} \hat{u}(\xi,t) e^{2\pi i \xi x}. \tag{3}$$

Derivatives are treated in Fourier space where they are multipliers and a fast Fourier transform (FFT) is used to pass between physical space and Fourier space as needed. The resulting system of ordinary differential equations for the Fourier coefficients is solved using a finite difference time stepper; typically this system of ordinary differential equations is solved in Fourier space to enable the treatment of terms which are linear in Fourier space exactly through the use of an integrating factor.

A detailed description of the generalization of this approach to stochastic partial differential equations such as Eq. (2) is given in [52]. Here, the discussion will focus on those aspects of the scheme that are unique to the stochastic system while only considering the simplest possible version of the spectral methods. In particular, the spectral treatment of the multiplicative noise term in Eq. (2) and the use of a suitable time discretization technique will be discussed briefly here.

A. Treatment of noise term

A crucial step in the development of a spectral scheme for a stochastic partial differential equation such as Eq. (2) is to obtain a spectral representation for the spatial component of the noise term. It is well known [54] that a stationary, isotropic, Gaussian random field $v(x)$ can be represented by the following stochastic integral in Fourier space:

$$v(x) = \int e^{2\pi i x \xi} S^{1/2}(\xi) dW(\xi), \tag{4}$$

where W is Brownian motion and S is the spectral density function of the random field v. Consistent numerical schemes for the simulation of random fields are based upon discretizations of this stochastic integral [55–61]. The simplest such discretization uses equispaced nodes and is known as the Fourier method since this discretization results in what is essentially a Fourier series. This approximation can be written as

$$v(x) \approx \sum_{j=1}^{M} a_j \cos(2\pi\xi_j x) + b_j \sin(2\pi\xi_j x), \tag{5}$$

where a_j and b_j are independent Gaussians with mean zero and variance $S(\xi_j)\Delta\xi$. Due to the periodicity of the approximation in Eq. (5), the Fourier method is not suitable in applications in which the desired random field has long range correlations [55–58]. However, since the random field that is needed for the numerical study of Eq. (2) lacks long range correlations, the Fourier method should be suitable. The Fourier method is also computationally attractive since an FFT can be used directly to evaluate Eq. (5) at all physical space lattice sites.

The approximation in Eq. (5) is used to represent the spatial component of the noise. Since each realization of the noise at a given time is essentially a Fourier series, the noise term in Eq. (2) can be calculated by completing all multiplications in physical space and all differentiations in Fourier space, using the FFT to pass back and forth between physical space and Fourier space as necessary. In other words, the existence of the Fourier series representation of the noise in Eq. (5) allows for the treatment of the stochastic term in the same fashion as in deterministic spectral methods.

B. Time discretization

Using the above approach for the spatial components, the solution of the stochastic partial differential equation in Eq. (2) effectively has been reduced to the solution of a system of stochastic ordinary differential equations where the unknowns are the Fourier coefficients in Eq. (3). Any one of these stochastic ordinary differential equations can be written in Ito form as

$$du = a(u)dt + b(u)dW(t), \tag{6}$$

where a is the drift coefficient and b is the diffusion coefficient to use the standard terminology from the stochastic ordinary differential equations literature [62]. Since numerical schemes that were derived for deterministic ordinary differential equations do not include the stochastic corrections from the Ito calculus, it is inadvisable to use them directly in the stochastic setting. For example, the deterministic Euler method applied to a stochastic ordinary differential equation has a strong (pathwise) order of convergence of $\frac{1}{2}$ rather than order 1 as in the deterministic setting [62]. Thus it is essen-

tial to use schemes that are derived directly from suitable truncations of Taylor-Ito series rather than deterministic Taylor series. However, such schemes typically include derivatives of the drift and the diffusion coefficients. Given the nonlinearity of these terms in Eq. (2) and the fact that time steps are being taken in spatial Fourier space, it is useful to use derivative-free Runge-Kutta type schemes [62–64]. One choice of a first order strong scheme for Eq. (6) is the following:

$$u_{n+1} = u_n + a(u_n)\Delta t + b(u_n)\Delta W_n + \frac{1}{2\sqrt{\Delta t}}[b(\tilde{u}_n) - b(u_n)] \times [(\Delta W_n)^2 - \Delta t] \tag{7}$$

with supporting value $\tilde{u}_n$ given by

$$\tilde{u}_n = u_n + b(u_n)\sqrt{\Delta t}, \tag{8}$$

where ΔW_n is a Gaussian with mean 0 and variance Δt. Since the solution of Eq. (2) is real, it is required that the Fourier coefficients in Eq. (3) respect the symmetries that are present in spectral representations of real fields, i.e., $\hat{u}(\xi,t) = \hat{u}(-\xi,t)$ where the overline denotes complex conjugate. Since the time steps are being completed in Fourier space, it is essential that the ΔW_n's used maintain this symmetry.

C. Computational verification of method

Computational evidence of the validity of the simulation method described above is given in [52]. In that work, stochastic partial differential equations for which one can analytically obtain the equilibrium covariance are considered as computational benchmark problems. These benchmark problems included equations with additive noise and multiplicative noise; in fact, one of these equations has a noise term of the same form as the noise term in Eq. (2). In [52], good agreement was exhibited between simulation results and analytic results for a wide variety of choices of spectral density function S that would be appropriate approximations for white noise, including the most straightforward choice of $S(\xi)=1$. Thus this choice was used to obtain all of the simulation results presented in this paper. While all the results in [52] were shown for 5000 realizations in order to insure negligible sampling error, results having errors typically less than 3% were obtained when only 500–1000 realizations were used.

IV. SIMULATION RESULTS

Some simulation results for the mesoscopic model in Eq. (2) using the spectral method discussed above in Sec. III are now given. To begin, we demonstrate the qualitative behavior that is observed in this system and then briefly describe some of the quantitative results that appeared in [37] in order to motivate the use of the special configuration which is the main topic of this section. Figure 1 contains contour plots of a single realization of simulation results for Eq. (2) at times 3, 5, 7, and 9. Lighter shades correspond to higher concentrations while darker shades correspond to lower concentrations. The migration potential in Eq. (2) was chosen to be

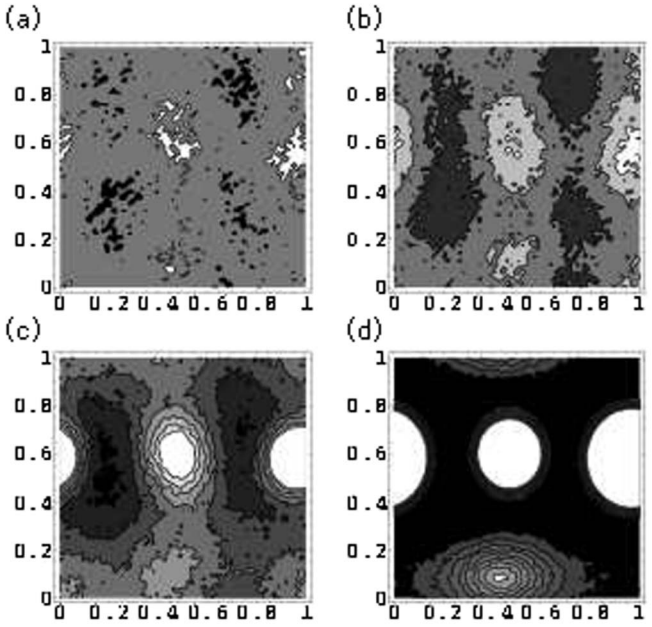

FIG. 1. Contour plots demonstrating the time evolution of the concentration field obtained from mesoscopic simulations of Eq. (2) for the choice of interaction parameter $r_0=0.05$ at times (a) $t=3$, (b) $t=5$, (c) $t=7$, and (d) $t=9$. The lighter shades represent regions of higher concentration while the darker shades represent regions of lower concentration. The expected self-organization into regions of high concentration is observed.

$$J_m(x) = \frac{1}{\sqrt{\pi r_0^2}} \exp\left(\frac{-|x|^2}{r_0^2}\right) \tag{9}$$

with $r_0=0.05$ being the parameter that describes the interaction length. The other parameters in Eq. (2) are chosen to be $D=0.1$, $\beta=6$, and $\gamma=r_0^2$. Simulation parameters include 64 wave numbers in each direction and a step size of $\Delta t = 0.000\,01$; this time step insures numerical stability of the time stepping scheme in Eqs. (7) and (8). The domain of the computation is a unit square with periodic boundary conditions. The system is initialized so that $\langle u(x,0)\rangle=0.25$ with small amplitude perturbations about this mean. At the earliest time shown in Fig. 1, the formation of several small regions of high and low concentration is observed. At later times, the number of regions of high concentration decreased while the size of the remaining regions increased. Eventually only one circular region of high concentration remained at later times than those depicted in Fig. 1. These results are in good agreement with physical intuition and experimental observations in such situations: In order to minimize free energy, the system evolves by minimizing the curvature of the regions of high concentration resulting in fewer of these regions of larger average size.

In [37], this self-organization was quantified by computing the typical domain size and making comparisons with the LSW theory. The computation of the typical domain size was completed using the standard approach [23,25,65] based upon the radially averaged covariance and spectral density function of the concentration field. Since the covariance and

spectral density function are a Fourier transform pair, the typical length of the concentration field corresponds to the maximum value of the spectral density function. However, this maximum is difficult to calculate numerically; the mean of the spectral density function is used as the measure of the typical length scale of the system.

As reported in [37], the typical domain size exhibited growth comparable with the LSW law in Eq. (1) at earlier times in simulation of Eq. (2), while growth with a larger exponent was observed at later times. However, the lack of radial symmetries in the concentration field depicted in Fig. 1 indicate the difficulty in using this approach to measure typical domain size beyond time 3 in this case. Also when the system consists of a low concentration background with circular regions of high concentration, the regions of low concentration will make significant contributions to the covariance of the concentration field thereby diminishing the effectiveness of this quantity as a measure of the size of the high concentration regions. Calculating the mean value of the spectral density function in each direction without radial averaging is also problematic in that unidirectional covariances can greatly underestimate or overestimate correlation lengths, especially when the underlying field has a striped structure. Thus difficulties in the measurement of the typical size of the high concentration regions prevented longer time quantitative studies of Ostwald ripening; the limitation was not caused by the simulation algorithm or the complexity of the model.

In order to study the long time behavior of this system, the time evolution of the concentration field when starting from a special configuration which serves as a caricature for the late stages of self-organization is considered here. The study of self-organization from special initializations of the concentration field has been used before with a variety of models and computational techniques by many authors [15,17,66,67]. Here, an initial concentration field consisting of two circular regions is used since configurations of this nature are observed in the late stages of self-organization. [Observe the system at time 9 in Fig. 1(d) has essentially reduced to such a configuration.] For the simulation results described in the remainder of this section, these two circular regions of high concentration are placed in a unit square with centers separated by a distance of 0.5 along the vertical axis. Periodic boundary conditions are used. The regions of high concentration are connected to the surrounding regions of low concentration using rapidly decaying exponentials. The upper circle is initialized to have a radius of 0.1 while the lower circle has the slightly smaller initial radius of 0.09. At early times, the system relaxes to circular regions with greater extent than initially with a less steep connection between regions of low concentration and high concentration. These start up effects are not depicted on the plots given in this section.

Figure 2 contains contour plots of a typical single realization of concentration field obtained via simulation of Eq. (2) using the spectral scheme described in Sec. III for the case $r_0=0.06$ for times 0.01, 5, 6, 7, 9, 10. These times were selected to be representative of the behavior observed in the system. The light areas represent regions of high concentration while the dark areas represent regions of low concentration. The contours are centered about a concentration of 0.5 with contours spaced 0.15 apart. Other parameters are chosen as in Fig. 1: 64 wave numbers in each direction, $D=0.1$, $\beta=6$, $\gamma=r_0^2$, and $\Delta t=0.000\,01$. As expected based upon physical intuition, the smaller lower region of high concentration eventually disappears leaving a single region of higher concentration. During this evolution, the smaller region appears to remain very nearly circular while the larger, growing region appears to be elliptical until eventually returning to a circular shape.

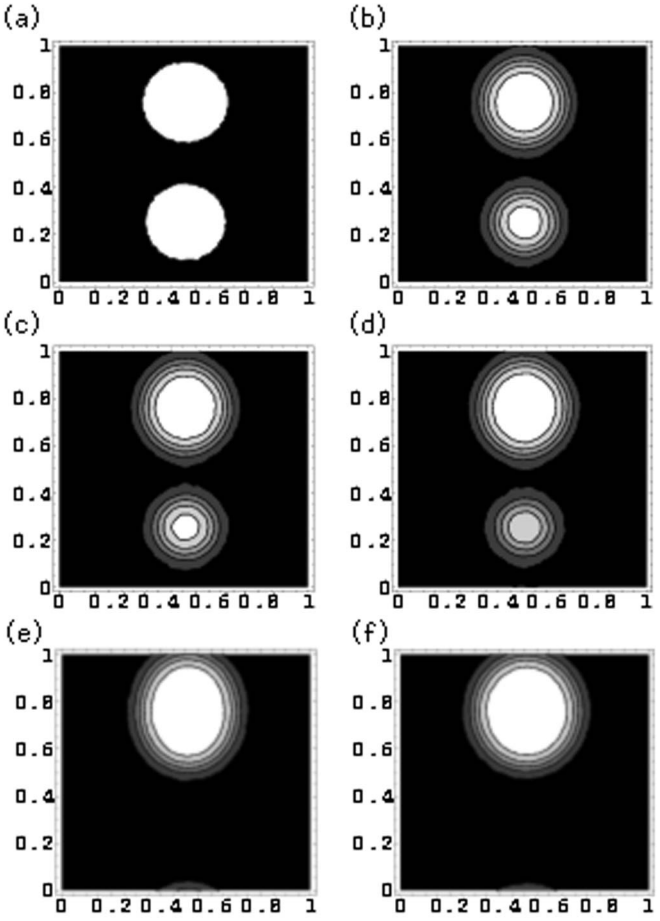

FIG. 2. Contour plots demonstrating the time evolution of the concentration field for the special initial configuration for the interaction parameter $r_0=0.06$ at times (a) $t=0.01$, (b) $t=5$, (c) $t=6$, (d) $t=7$, (e) $t=9$, and (f) $t=10$. At intermediate times, the regions become elliptical in shape. The lower region eventually disappears as expected.

Quantifying the behavior observed in Fig. 2 is useful in understanding this phenomenon. In this special geometry, this size of each region can be directly measured; the boundary of the region is selected to be the location where the concentration field takes the value of 0.5. Linear interpolation is used to calculate the boundary points that are located between grid points. Figure 3 depicts the time evolution of the horizontal and vertical diameters of the regions of high concentration after averaging over 750 realizations. The darker lines correspond to the larger, upper region and the lighter lines correspond to the smaller, lower region. The lower region deviates slightly from circular whereas the up-

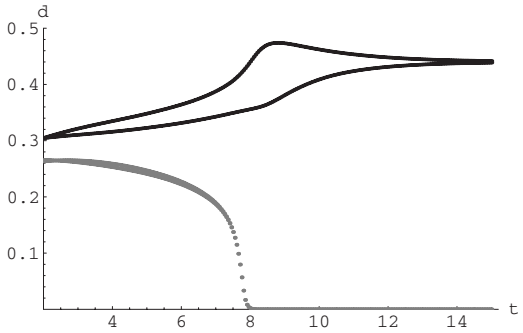

FIG. 3. Plots of the time evolution of the major and minor axes of the two elliptical regions of high concentration. The darker lines correspond to the upper, larger region of high concentration while the lighter lines correspond to the lower, smaller region of high concentration. The greater deformation from circular in the upper region can clearly be seen in this plot.

per region becomes quite elliptic near the time when the lower region disappears and eventually becomes circular again. These results are as expected given the behavior observed in Fig. 2 for a single realization.

Figure 4 depicts the time evolution of the area of each of the regions of high concentration for the same parameter values as Fig. 3. The upper curve corresponds to the upper, larger region while the lower curve corresponds to the lower, smaller region. This figure also demonstrates the very rapid change in the larger region of high concentration immediately following the disappearance of the lower region.

Figure 5 shows the effective radius of the regions of high concentration as a function of time. The effective radius is calculated to be the radius of the circle which has the same area as each of the (elliptic) regions of high concentration. The effective radius showed the same qualitative behavior as observed for the area and the major and minor axes of the elliptic regions. However, the effective radius is an important quantity to consider because it is most like the typical domain size of the LSW theory for self-organization. The effective radius of the larger region does not demonstrate power law growth, even at the earlier times depicted in Fig. 5. Compared with the $t^{1/3}$ of the LSW theory, the growth observed in the effective radius of the larger region is much

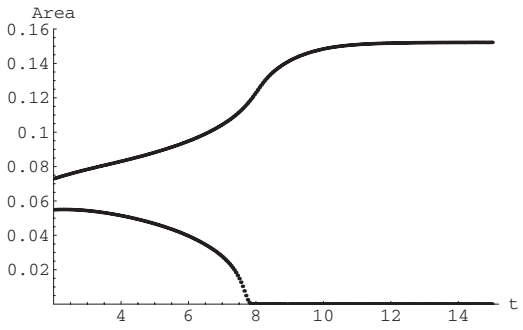

FIG. 4. Plots of the time evolution of the area of the upper and lower regions of high concentration. The upper line corresponds to the upper, larger region while the lower line corresponds to the lower, smaller region. The very rapid growth of the upper region as the lower region disappears is quite evident in this plot.

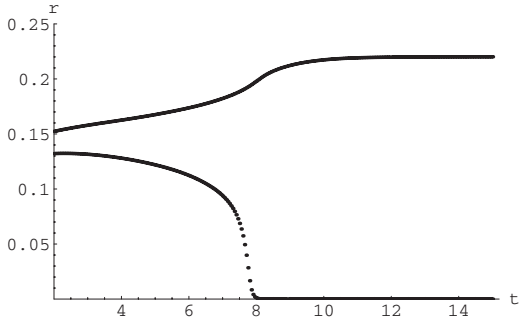

FIG. 5. Plots of the time evolution of the effective radius of the upper and lower regions of high concentration. The upper line corresponds to the upper, larger region while the lower line corresponds to the lower, smaller region. The effective radius is most like the typical length scale of the LSW (Lifshitz, Slyozov, Wagner) growth law; however, power law behavior is not observed.

slower. The slow, non-power-law growth was also observed in the direct average of the effective radii of both regions as well as the average weighted by the respective areas of each region. Slower growth is what would be expected to eventually occur as the final state is reached since growth can no longer occur once the system has organized into a single circular region. These results would imply that when a self-organizing system has reached the two circle regime it is already beyond any regime in which a scaling law such as the LSW growth law could hold.

It is also interesting to observe the effect of changing the interaction length r_0 in Eq. (9) on the late stages of self-organization. Intuitively, one would expect that the evolution of the system would be faster in the presence of longer range interactions since greater interaction lengths facilitate the location of like particles or phases. Figure 6 contains the major and minor axes of the upper and lower regions of high concentration for the choice of $r_0=0.05$. Comparing with Fig. 3 for $r_0=0.06$, a much slower evolution is observed, with the lower region not disappearing until just before $t=15$ rather than $t=8$ in Fig. 3, as is intuitively expected. All of the other qualitative features of coarsening already discussed for the

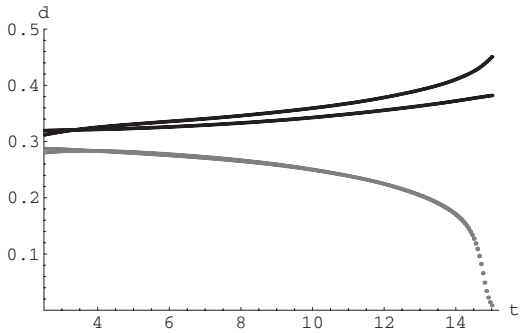

FIG. 6. Plots of the time evolution of the major and minor axes of the two elliptical regions of high concentration for the choice $r_0=0.05$. The darker lines correspond to the upper, larger region of high concentration while the lighter lines correspond to the lower, smaller region of high concentration. When compared with Fig. 3 ($r_0=0.06$), slower evolution is observed, as would be expected in situations with smaller interaction lengths.

$r_0=0.06$ earlier are also observed in this case. Thus the plots analogous to Figs. 4 and 5 are not included here for the sake of brevity.

Many other configurations similar to those discussed above were also considered. When the relative difference in the size of the initial circular regions was greater, the smaller circular region disappeared more rapidly; however, the larger region still exhibited slower growth than predicted by the LSW theory and also did not grow like a power law. Likewise, initializing the system with two circular regions of more comparable size resulted in a much slower disappearance of the smaller circular region. For the sake of brevity, these results are not shown given the qualitative and quantitative similarity to the results already included.

V. SUMMARY

This paper has demonstrated the value of the mesoscopic modeling approach used in conjunction with a spectral simulation scheme for stochastic partial differential equations to study self-organization. Prior analytic work [39,40] and computational work [37] have indicated the validity of the mesoscopic model. In the mesoscopic simulation study in [37], a regime of growth in a self-organizing system from a random initial configuration was observed to behave according to the LSW theory. In order to study the late stages of self-organization, a system with a simple geometry consisting of two circular regions of high concentration in a low concentration background was studied using mesoscopic simulation. This special geometry is similar to that observed in the late stages of coarsening from a random initial configuration. Such a special initial configuration allows for the direct measurement of domain sizes, which is important due to symmetry assumptions in the commonly used measures of typical domain size in self-organizing systems. In these simulations, power law growth in the domain size was not observed before, during, or after the rapid change in domain size that occurred when the smaller region diffused away, thereby indicating such configurations are beyond any regions in which scaling laws for growth hold. Longer interaction lengths resulted in faster self-organization in these simulations; this behavior is reasonable as longer interaction lengths would be expected to facilitate the location of like particles.

Further studies of the long time behavior of the self-organizing system are warranted. The effect of the boundary conditions is obviously very worthy of study and will require the development of alternative versions of the spectral scheme that was briefly described here. Given the ease in which different sorts of particle interactions can be used in mesoscopic models, there are many additional classes of interaction potentials which should be considered. Anisotropic potentials would be useful in coarsening systems in which there is a preferred direction for growth. Potentials with repulsive interaction ranges would naturally arise in systems with charged particles.

ACKNOWLEDGMENTS

The author would like to thank Markos Katsoulakis for many useful conversations. This research was partly supported by NSF Grants No. DMS-0219211, No. DMS-0406633, and No. DMS-0420590 (MRI-computer cluster).

[1] I. Lifshitz and V. Slyozov, J. Phys. Chem. Solids **19**, 35 (1961).
[2] C. Wagner, Z. Elektrochem. **65**, 581 (1961).
[3] M. Newman and G. Barkema, *Monte Carlo Methods in Statistical Physics* (Clarendon Press, Oxford, 1999).
[4] O. Penrose, in *Material Instabilities in Continuum Mechanics and Related Mathematical Problems*, edited by J. Ball (Clarendon Press, Oxford, 1988), p. 373.
[5] P. Voorhees, J. Stat. Phys. **38**, 231 (1985).
[6] P. Voorhees, Annu. Rev. Mater. Sci. **22**, 197 (1992).
[7] J. Yao, K. Elder, H. Guo, and M. Grant, Physica A **204**, 770 (1994).
[8] P. Voorhees and R. Schaefer, Acta Metall. **35**, 327 (1987).
[9] J. Lebowitz, E. Orlandi, and E. Presutti, J. Stat. Phys. **63**, 993 (1991).
[10] M. Katsoulakis and P. Souganidis, J. Stat. Phys. **87**, 63 (1997).
[11] M. Hildebrand and A. S. Mikhailov, J. Phys. Chem. **100**, 19089 (1996).
[12] G. Giacomin and J. Lebowitz, Phys. Rev. Lett. **76**, 1094 (1996).
[13] D. Horntrop, M. Katsoulakis, and D. Vlachos, J. Comput. Phys. **173**, 364 (2001).
[14] G. McFadden, P. Voorhees, R. Boisvert, and D. Meiron, J. Sci. Comput. **1**, 117 (1986).
[15] P. Voorhees, G. McFadden, R. Boisvert, and D. Meiron, Acta Metall. **36**, 207 (1988).
[16] N. Akaiwa and D. Meiron, Phys. Rev. E **54**, R13 (1996).
[17] T. Imaeda and K. Kawasaki, Physica A **186**, 359 (1992).
[18] T. Hou, J. Lowengrub, and M. Shelley, J. Comput. Phys. **169**, 302 (2001).
[19] F. Filbet and P. Laurençot, SIAM (Soc. Ind. Appl. Math.) J. Numer. Anal. **41**, 563 (2003).
[20] J. Carrillo and T. Goudon, J. Sci. Comput. **20**, 69 (2004).
[21] C. Elliott and D. French, SIAM (Soc. Ind. Appl. Math.) J. Numer. Anal. **26**, 884 (1989).
[22] J. Barrett and J. Blowey, Math. Comput. **68**, 487 (1999).
[23] A. Chakrabarti, R. Toral, and J. Gunton, Phys. Rev. E **47**, 3025 (1993).
[24] J. Gunton, R. Toral, and A. Chakrabarti, Phys. Scr. **T33**, 12 (1990).
[25] T. Rogers, K. Elder, and R. Desai, Phys. Rev. B **37**, 9638 (1988).
[26] T. Rogers and R. Desai, Phys. Rev. B **39**, 11956 (1989).
[27] E. de Mello and O. Filho, Physica A **347**, 429 (2005).
[28] Y. Oono and S. Puri, Phys. Rev. A **38**, 434 (1988).
[29] S. Puri, A. Bray, and J. Lebowitz, Phys. Rev. E **56**, 758 (1997).
[30] K. Kawasaki, Phys. Rev. **145**, 224 (1965).

[31] J. Gunton, E. Gawlinski, and K. Kaski, in *Dynamics of Ordering Processes in Condensed Matter*, edited by S. Komura and H. Furukawa (Plenum, New York, 1988), p. 101.
[32] D. Landau and K. Binder, *A Guide to Monte Carlo Simulations in Statistical Physics* (Cambridge University Press, Cambridge, England, 2000).
[33] S. van Gemmert, G. Barkema, and S. Puri, Phys. Rev. E **72**, 046131 (2005).
[34] B. Zheng, Int. J. Mod. Phys. B **12**, 1419 (1998).
[35] M. Katsoulakis and D. Vlachos, J. Chem. Phys. **119**, 9412 (2003).
[36] M. Katsoulakis, A. Majda, and D. Vlachos, J. Comput. Phys. **186**, 250 (2003).
[37] D. Horntrop, J. Comput. Phys. **218**, 429 (2006).
[38] D. Horntrop, in *Computational Science-ICCS 2005*, edited by V. Sunderam *et al.* (Springer, Berlin, 2005), p. 852.
[39] D. Vlachos and M. Katsoulakis, Phys. Rev. Lett. **85**, 3898 (2000).
[40] R. Lam, T. Basak, D. Vlachos, and M. Katsoulakis, J. Chem. Phys. **115**, 11278 (2001).
[41] J. Gaines, in *Stochastic Partial Differential Equations*, edited by A. Etheridge (Cambridge University Press, Cambridge, England, 1995), p. 55.
[42] I. Gyöngy, in *Stochastic Partial Differential Equations and Applications*, edited by G. Da Prato and L. Tubaro (Marcel Dekker, New York, 2002), p. 287.
[43] I. Gyöngy and N. Krylov, Ann. Probab. **31**, 564 (2003).
[44] M. Seesselberg and F. Petruccione, Comput. Phys. Commun. **74**, 303 (1993).
[45] H. Yoo, Math. Comput. **69**, 653 (2000).
[46] R. Ghanem and P. Spanos, *Stochastic Finite Elements: A Spectral Approach* (Springer, New York, 1991).
[47] E. Allen, S. Novosel, and Z. Zheng, Stoch. Stoch. Rep. **64**, 117 (1998).
[48] I. Babuška, R. Temponet, and G. Zouraris, SIAM (Soc. Ind. Appl. Math.) J. Numer. Anal. **42**, 800 (2004).
[49] M. Deb, I. Babuška, and J. Oden, Comput. Methods Appl. Mech. Eng. **190**, 6359 (2001).
[50] Q. Du and T. Zhang, SIAM (Soc. Ind. Appl. Math.) J. Numer. Anal. **40**, 1421 (2002).
[51] L. Machiels and M. Deville, J. Comput. Phys. **145**, 246 (1998).
[52] D. Horntrop (unpublished).
[53] C. Canuto, M. Hussaini, A. Quarteroni, and T. Zang, *Spectral Methods in Fluid Dynamics* (Springer, New York, 1988).
[54] J. Doob, *Stochastic Processes* (Wiley, New York, 1953).
[55] F. Elliott, A. Majda, D. Horntrop, and R. McLaughlin, J. Stat. Phys. **81**, 717 (1995).
[56] F. Elliott, D. Horntrop, and A. Majda, Chaos **7**, 39 (1997).
[57] F. Elliott, D. Horntrop, and A. Majda, J. Comput. Phys. **132**, 384 (1997).
[58] D. Horntrop and A. Majda, in *Monte Carlo Simulations in Oceanography, Proceedings of the 9th Aha Huliko Hawaiian Winter Workshop*, edited by P. Muller and D. Henderson (University of Hawaii, Honolulu, 1997), p. 67.
[59] S. Prigarin, *Spectral Models of Random Fields in Monte Carlo Methods* (VSP, Utrecht, 2001).
[60] K. Sabelfeld, *Monte Carlo Methods* (Springer, Berlin, 1991).
[61] P. Kramer, O. Kurbanmuradov, and K. Sabelfeld (unpublished).
[62] P. Kloeden and E. Platen, *Numerical Solution of Stochastic Differential Equations* (Springer, Berlin, 1992).
[63] K. Burrage and E. Platen, Ann. Numer. Math. **1**, 63 (1994).
[64] K. Burrage and P. Burrage, Appl. Numer. Math. **22**, 81 (1996).
[65] S. Glotzer, E. Di Marzio, and M. Muthukumar, Phys. Rev. Lett. **74**, 2034 (1995).
[66] T. Imaeda and K. Kawasaki, Mod. Phys. Lett. B **3**, 207 (1989).
[67] T. Imaeda and K. Kawasaki, Physica A **164**, 335 (1990).